ORIGINAL CONTRIBUTION

Stepwise strain-induced crystallization of soft composites prepared from natural rubber latex and silica generated in situ

Yuko Ikeda · Atitaya Tohsan

Abstract Novel biphasic structured in situ silica filled natural rubber composites were focused on their strain-induced crystallization (SIC) behavior from the viewpoint of morphology. The composites were prepared by in situ silica filling in natural rubber (NR) latex using a sol–gel reaction of tetraethoxysilane. Simultaneous time-resolved wide-angle X-ray diffraction and tensile measurements revealed a relationship between the characteristic morphology and tensile stress–strain properties of the composites associating with the SIC. Results showed stepwise SIC behaviors of NR-based composites for the first time. Pure rubber phases in the biphasic structure were found to afford highly oriented amorphous segments and oriented crystallites. The generated crystallites worked as reinforcing fillers together with the in situ silica to result in high tensile stresses of the composites. The observed characteristics are useful for understanding a role of filler network in the reinforcement of rubber.

Keywords Natural rubber · In situ silica · Strain-induced crystallization · Time-resolved WAXD · Stepwise

Introduction

Natural rubber (NR) has been widely recognized as a useful soft mater, which is both highly elastic and crystallizable under high strains [1–3]. NR is indispensable for manufacturing pneumatic tires of heavy-duty uses, e.g., those for aircrafts, heavy trucks, and rubber bearings in a seismic isolation system [1–4]. Thin NR films, which are directly prepared from NR latex without coagulation, are also very important materials for

Y. Ikeda (✉) · A. Tohsan
Graduate School of Science and Technology, Kyoto Institute of Technology, Matsugasaki, Sakyo, Kyoto 606-8585, Japan
e-mail: yuko@kit.ac.jp

biomedical and health care fields [1, 5, 6]. These extensive applications of NR are based on its high elasticity and excellent mechanical strength. The latter is ultimately attributable to its ability of crystallization upon stretching [1–4, 7–11]. Therefore, it is necessary to evaluate the strain-induced crystallization (SIC) behavior for development of high performance NR materials.

Up to now, the SIC behavior of NR have been extensively studied [7–20]. The research group of one of the authors has also carried out studies on the SIC not only for cross-linked NR [16–19] but also for filler-filled cross-linked NR [21–23]. A general tendency of the SIC behavior of NR was thus established [16–19]: Upon tensile deformation, polymer chains start to be stretched. Among the polymer chains, short ones are fully stretched first, and these fully-stretched chains can act as precursors for crystallization like a nucleus of crystallites. Therefore, the NR crystallites are usually observed to grow up in the direction perpendicular to the molecular chain axis [22, 23]. Upon stretching, the generation of crystallite is generally found to be linearly increased in cross-linked NR samples. Since the distribution of network chain length is not monodispersed, the SIC behavior depends on the heterogeneity of cross-linked rubber [19, 24], which is significantly related with cross-linking systems such as sulfur or peroxide cross-links. In addition, the nonuniformity of NR also affects the SIC due to the presence of nonrubber components, as it was proved by atomic force microscopy and small-angle neutron scattering analyses [25, 26].

Reinforcing fillers, on the other hand, have been known to be of remarkable influence on the SIC of NR because of their strong interfacial interactions with the polymer matrix. Studies on the SIC behavior of carbon black/NR composites have been especially focused due to the importance for heavy-duty uses [21, 22, 27–30]. Among these studies, there are some common observations: By the inclusion of carbon black, a start of SIC shifted to a lower strain, i.e., the SIC was apparently accelerated.

This tendency was, however, at least partially explained due to the decrease of volume fraction of NR in the material by the isotropic filler inclusion. In terms of crystallinity, it was commonly observed to linearly increase with an increase in strain similarly with nonfilled NR. These phenomena were also detected in commercial silica filled NR-based composites [29] and in situ silica filled one [23].

Recently, we prepared novel biphasic structured in situ silica filled NR composites by a sol–gel reaction of tetraethoxysilane using n-butylamine in NR latex [31]. This preparation procedure is a kind of soft process as the composites were prepared by liquid-state mixing and followed by casting to obtain thin films. In the composites, the in situ silica was locally dispersed around rubber particles to result in the specific morphology. Namely, NR particles in the latex worked as templates to form the novel biphasic structure in the composites. The rubber phase in the biphasic structure was of higher purity than that of the composite prepared by conventional mechanical mixing. Thus, unique dynamic mechanical properties were detected in the composites. In order to further clarify the characteristics of the biphasic structured in situ silica filled NR composites, the simultaneous synchrotron wide-angle X-ray diffraction (WAXD) and tensile measurements were conducted in this study. Nowadays, in situ generated silica in a rubbery matrix moves forward into the nanotechnology [32–34]. Therefore, present results will be useful for further developing of rubber-based nanocomposites.

Experimental

Materials

Sulfur cross-linked and uncross-linked in situ silica filled NR composites were used in this study, which were prepared by the soft processing method [31]. The former and the latter are abbreviated as S-NR-Si and NR-Si, respectively. Their in situ silica contents were 10 phr. An unfilled sulfur cross-linked NR film (S-NR) was similarly prepared [31] and used as a reference sample. All specimens subjected to the measurements in this study were virgin samples.

Images of transmission electron microscopy (TEM) for S-NR-Si and NR-Si are displayed in Fig. 1 [31]. Dark phases show the generated in situ silica. The TEM photographs did not clearly give us a definite size of in situ silica particles, but the silica was observed to more or less aggregate in the composites. It is worth noting that the in situ silica was dispersed around the rubber phases (the bright phases in the photographs), and there was little silica inside the rubber phases. Therefore, the characteristic morphology of in situ silica may be a model of a filler network in the rubber matrix. The filler network seems to be fallen into different sizes, which is ascribable to different sizes of NR particles in the latex.
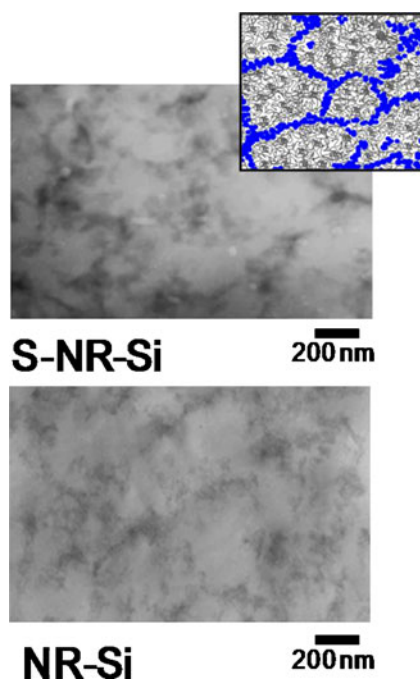

Fig 1 TEM photographs of the in situ silica filled NR composites. Reprinted in part with permission from [31]. Copyright 2011 John Wiley & Sons, Ltd

Measurement of density

A density of the sample was measured using Shimadzu Unibloc Analytical Balances. The experiment was carried out at 25 °C using ethanol as a solvent. The density was calculated using Eq. 1 and summarized in Table 1.

$$\rho = \frac{W_a}{W_a - W_l} \rho_l \tag{1}$$

where W_a is a weight of the sample in air, W_l is a weight of the sample in the liquid, ρ_l is a density of the liquid, and ρ is a density of the sample.

Estimation of network-chain density

A network-chain density (ν) of the cross-linked sample was estimated on the basis of the classical theory of rubber elasticity [9].

$$\sigma = \nu RT \left(\alpha - \frac{1}{\alpha^2} \right) \tag{2}$$

where σ is tensile stress, R is gas constant, α is stretching ratio ($\alpha = l/l_0$, l_0 and l are the initial length and the length after stretching of the sample, respectively), and T is absolute temperature.

Table 1 Properties of the samples

[a] Tensile strength at break.

[b] Elongation at break.

[c] Physical cross-linking density estimated by Eq. (2)

Sample code	Density (g/cm^3)	Poisson's ratio	Network chain density $\times 10^4$ (mol/cm^3)	Stress at $\alpha = 3$ (MPa)	Stress at $\alpha = 5$ (MPa)	T_B[a] (MPa)	E_B[b]
NR-Si	0.961	0.4991	1.7[c]	1.8	4.2	6.2	6.0
S-NR-Si	0.964	0.4932	3.4	3.4	6.2	8.1	6.1
S-NR	0.927	0.4983	2.9	1.0	1.8	25.1	9.3

Simultaneous wide-angle X-ray diffraction and tensile measurements

Simultaneous WAXD and tensile measurements were carried out using a synchrotron radiation system at BL-40XU beam line of SPring-8 in Harima, Japan [35]. A custom-made tensile tester (ISUT-2201, Aiesu Giken Co., Kyoto) was situated on the beam line, and WAXD patterns were recorded during the tensile measurement at room temperature (about 25 °C). The wavelength of the X-ray was 0.0832 nm, and the camera length was 198 mm. Two-dimensional WAXD patterns were recorded using a charge-coupled device (CCD) camera (ORCA II, Hamamatsu Photonics, Co.). Intensity of the incident X-ray was attenuated using a rotating slit equipped on the beam line, and the incident beam was exposed on the sample for 40 ms every 3 s. The intensities of the incident beam and transmitted beam through air were measured using ion chambers. A ring-shaped sample was subjected to the tensile measurement in order to correctly measure the stretching ratio (α) of deformed sample. The stretching speed was 100 mm/min, i.e., strain speed was about 4.98/min. An absorption correction for thinning of the sample under stretching was carried out using calculated correction coefficients, which were estimated on the basis of absorption coefficients per density [36] and weight fractions of each element in the sample. Here, an affine deformation was assumed for all rubber samples on the basis of their measured Poisson's ratios. The Poisson's ratio was measured separately under the similar experimental condition with that of simultaneous WAXD and tensile measurements using a CCD camera (VC1000 Digital Fine Scope, OMRON Co.). The measured values of Poisson's ratio are listed in Table 1.

WAXD analysis

The obtained WAXD images were processed using the software "POLAR" (Stonybrook Technology & Applied Research, Inc.) [15]. Each WAXD pattern of stretched sample was decomposed into three components, i.e., isotropic, oriented amorphous, and crystalline components. Three components were azimuthally integrated within the range of ±75° from the equator; the details of this analytical method were described in our previous papers [16, 17]. Two structural parameters were estimated at first, of which "crystallinity index" (CI) and

"oriented amorphous index" (OAI) are defined by the following equations.

$$\mathrm{CI} = \frac{\sum\limits_{\mathrm{crystal}} 2\pi \int \sin\phi d\phi \int I(s)s^2 \mathrm{d}s}{\sum\limits_{\mathrm{total}} 2\pi \int \sin\phi d\phi \int I(s)s^2 \mathrm{d}s} \qquad (3)$$

$$\mathrm{OAI} = \frac{\sum\limits_{\mathrm{oriented\ amorphous}} 2\pi \int \sin\phi d\phi \int I(s)s^2 \mathrm{d}s}{\sum\limits_{\mathrm{total}} 2\pi \int \sin\phi d\phi \int I(s)s^2 \mathrm{d}s} \qquad (4)$$

By summation of CI and OAI, the oriented index (OI) can be obtained as shown in Eq. 5

$$\mathrm{OI} = \mathrm{CI} + \mathrm{OAI} \qquad (5)$$

In Eqs. 3 and 4, $I(s)$ represents the intensity distribution of each peak that is read out from the WAXD pattern, s is the radial coordinate in reciprocal space in nm^{-1} unit [$s = 2(\sin\theta/\lambda)$, where λ is the wavelength and 2θ is the scattering angle], and ϕ is the angle between the scattering vector of the peak and the fiber direction. Figure 2 displays an example of peak fitting of the radial intensity distribution which obtained from a WAXD pattern of S-NR-Si. The peak fitting leads to the numerators of Eqs. 3 and 4. As seen in this image, we can clearly distinguished the content of crystallite segments at $s \approx$ 1.6, 2.0, 2.4, 2.7, and 3.0 which are corresponding to crystal planes of 200, 201, 120, 121, and 002, respectively. The remained three broad peaks were then ascribed to oriented amorphous segments. For all WAXD data, similar fitting results were obtained and were subjected to the calculation of CI and OAI values.

Coherent lengths (apparent crystallite sizes) were estimated using the Scherrer equation (Eq. 6) [37].

$$L_{hkl} = K\lambda/(\beta\cos\theta) \qquad (6)$$

where L_{hkl} is an apparent crystallite size in the direction perpendicular to the (hkl) plane, and θ is the Bragg angle (half of the scattering angle). In this study, the value 0.89 was tentatively used for K [38]. The intensity distribution on the equator was extracted from the original WAXD pattern. Each peak was fitted with a linear background and a Gaussian
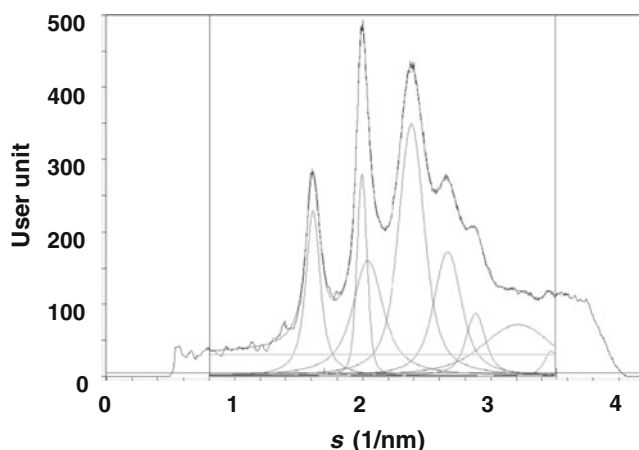
Fig. 2 One example of peak fittings, where the radial intensity distribution of S-NR-Si at $\alpha = 6$ is shown

function having the form $I(x) = h \exp[-(x-x_c)^2/(2w^2)]$, where $I(x)$ is the intensity at position (x). x_c is the position at the scattering maximum, and h and w are parameters related to the peak height and peak width, respectively[16, 17]. Each w value was converted into the half width (β).

Orientation fluctuations of 200 reflection were estimated from azimuthal scans of the peaks [16, 17]: The width parameter in the azimuthal direction (w_{az}) was obtained by fitting the intensity distribution with a Gaussian function. Then, the w_{az} was converted into the half width (β_{az}) by the following equation

$$\beta_{az} = 2w_{az} \sqrt{-2\ln(1/2)} \qquad (7)$$

Lattice constants (a, b, and c) were estimated from the WAXD patterns obtained during the deformation process using the least-squares regression method [16, 17]. The volume of unit cell was thus calculated using the a, b, and c values.

Results and discussion

Tensile characteristics of in situ silica filled NR composites prepared by the soft processing method

Tensile stress–strain curves up to mechanical rupture points of the in situ silica filled NR composites, i.e., S-NR-Si and NR-Si are shown in Fig. 3a with that of S-NR. Tensile stresses at $\alpha = 3$ and 5, tensile strength at break (T_B), and elongation at break (E_B) are summarized in Table 1 with other properties of the samples. Note that NR-Si was not chemically cross-linked but was physically cross-linked due to aggregation of nonrubber components in NR [25] and hydrogen-bonding between silica and rubber particles. The hydrogen-bonding is supposed to be mainly generated between carboxyl or amine groups in proteins of nonrubber components and silanol groups of silica particles.
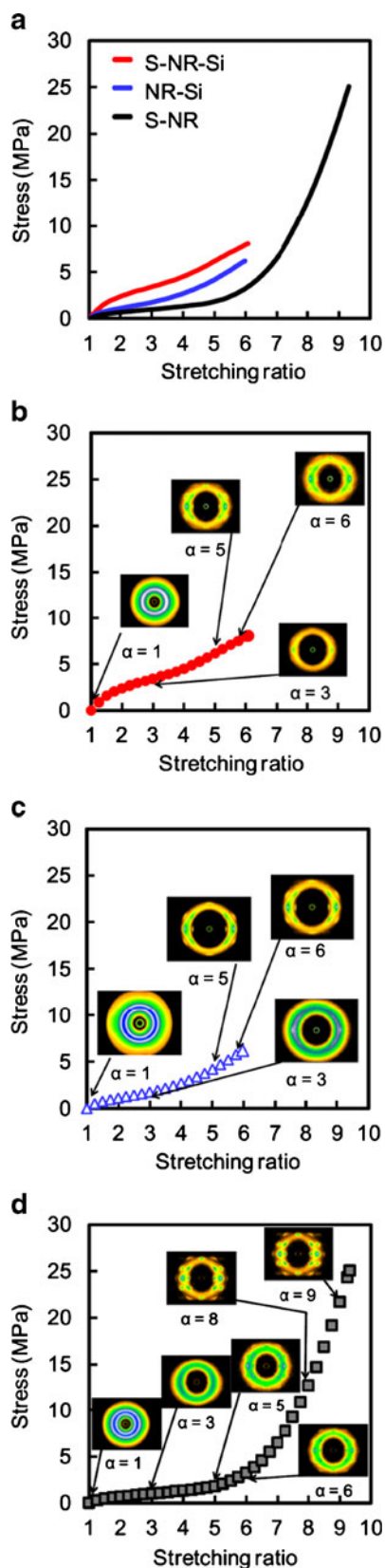

Fig. 3 Tensile stress–strain curves of the samples (**a**), WAXD images at stretching ratios of 1, 3, 5, 6, 8 and 9 showing SIC behaviours of S-NR-Si (**b**), NR-Si (**c**), and S-NR (**d**), respectively

It is clearly seen that the in situ silica filled composites, both cross-linked and uncross-linked ones, showed higher stresses than the unfilled sample up to stretching ratio of about 6. This is basically ascribable to reinforcement effect of the in situ silica. The sulfur cross-linking also increased the tensile stress of the in situ silica filled biphasic structured composite. For NR-based materials, an effect of SIC on the mechanical properties has to be also taken into account, because the strain-induced crystallites may play a role to increase the stress. Thus, simultaneous time-resolved WAXD and tensile measurements for these samples were carried out in situ in this study.

SIC of in situ silica filled NR composites prepared by the soft processing method

WAXD images at $\alpha = 1$, 3, 5, and 6 of the three samples are displayed in Fig. 3b–d together with their stress–strain curves. Plotted spots in the curves indicate events of X-ray irradiation in the WAXD measurements. For S-NR, WAXD images at $\alpha = 8$ and 9 are also displayed in Fig. 3d. Note that a background scattering by air was removed from their WAXD patterns. Initially, all samples showed only one broad ring at $\alpha = 1$, i.e., they were totally amorphous before stretching. The SIC started at $1 < \alpha < 3$ in the silica filled samples, while the unfilled sample was not yet crystallized at $\alpha = 3$ and its SIC was detected at high stretching ratio $3 < \alpha < 5$

It is also noted that the amorphous halo still remained even at the high stretching ratio in all samples, where strain-induced crystallites were generated already. Much earlier work by Katz also reported the presence of unoriented amorphous segments at high elongation [7]. Consequently, the remained large content of unoriented segments under the presence of strain-induced crystallites can be counted as a unique characteristic of polyisoprene chains under tensile deformation. Thus, it is estimated that the three states, i.e., completely amorphous segments, oriented amorphous segments, and oriented crystallites are coexisted in the samples. Thus, the WAXD results were subjected to the analysis to obtain three indexes, OI, OAI, and CI, according to the methods in "WAXD analysis." The results are shown in Fig. 4, respectively. Since silica particles do not deform upon stretching like rubber, an effective stretching ratio (α_e) was used for the comparison. It is defined by Eq. 8 [39],

$$\alpha_e = (\alpha - \gamma)/(1 - \gamma) \tag{8}$$

where γ is a volume fraction of filler. The density of in situ silica used for the calculation was 1.92 g/cm^3 [40–42]. In order to elucidate the effects of in situ silica filling and sulfur cross-linking on the SIC of the composites, strain dependences of OI, OAI, and CI are separately shown in Fig. 4a–c for S-NR-Si and S-NR and in Fig. 4d–f for S-NR-Si and NR-Si, respectively.

All SIC indexes show a tendency to increase with the increasing of strain. However, we observed unique behaviors

of SIC, i.e., "a stepwise SIC" for the in situ silica filled NR composites, which are distinguishably different with those of reported SIC phenomena as mentioned earlier [7–23, 27–30]. Thus, detailed discussions on the stepwise SIC are given in the following subsections.

Sulfur cross-linked in situ silica filled NR composite

As shown in Fig. 4a, short amorphous (assumed to be Gaussian) network chains of S-NR-Si began to orient immediately upon stretching. However, the OI did not increase linearly to the end, i.e., the OI repeated a small increase and a small decrease during the upward change. It is important to emphasize that the obtained results are reliable as we obtained a good reproducibility among three fittings for all parameters. Errors among the three fittings for each point were within ±0.8 % from the each average. Thus, the averages were plotted in the figures. The unique variation of the OI was also observed up to about 5 of α_e in the unfilled S-NR, but the up and down were much smaller and less frequent than those of the composite. The slope of the upward increase was steeper in S-NR-Si than in S-NR. At most of strain region, the OI was larger in S-NR-Si than in S-NR.

Strain dependences of *OAI* were very similar with those of OI as shown in Fig. 4b. The in situ silica filling in the NR latex was found to promote the orientation of NR chains to the stretching direction upon stretching. However, it is noted that the increase in OAI in S-NR-Si showed a few ark-like variations around 1.5, 2.5, and 3.5 of α_e. This observation suggests that the orientation of network chains was significantly restricted by the in situ silica in the biphasic structured soft composite. This consideration is supported by strain dependences of CI for S-NR-Si. As shown in Fig. 4c, three steps were detected in the variation of CI for S-NR-Si. Note that the region around 5.5 of α_e was judged as one step from the definitive change of orientation fluctuation of strain-induced crystallites (see "Relationship between SIC and tensile properties of in situ silica filled NR composites"). This unexpected variation of CI is ascribable to the specific morphology of the in situ silica filled biphasic structured composite as shown in Fig. 1a.

By comparing the variation of OAI with that of CI in S-NR-Si, two tendencies were observed: the OAI decreased at each plateau region of CI, and the OAI increased with the increase in CI. These two phenomena are explained as follows: In the cross-linked rubber phase of S-NR-Si, the short amorphous segments began to orient to the stretching direction upon stretching, and to result in the increase in OAI. Some of the oriented amorphous segments were crystallized by further stretching to increase the crystallinity. However, it became difficult for the amorphous segments to orient to the stretching direction due to the interruption of chain deformation by the silica layer around the rubber phase. Consequently, the progress of SIC became quite slow to give the plateau
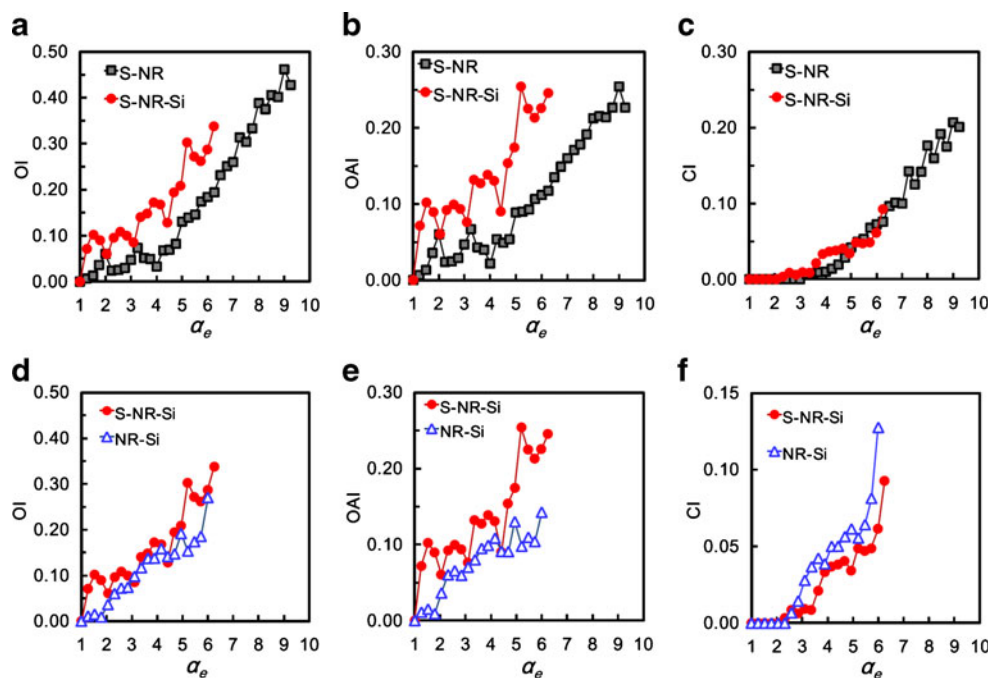
region. Once the silica layer was broken upon further stretching, however, the in situ silica particles must have been randomly dispersed into the rubbery matrix. Consequently, the rubber chains seemed to be freely extended to result in the acceleration of SIC. As a result, the OAI and CI increased again.

The speculated SIC behavior of S-NR-Si is schematically illustrated in Fig. 5 with a figure to show the variations of CI and OAI. The in situ silica phases are displayed by connected blue particles around the rubber phases, which are expressed by black lines. Black points in the rubber phases are cross-linking sites. Red lines are short rubber chains which connect the cross-linking sites: Before the deformation, the rubber chains are in coil state as shown in Fig. 5b. When the deformation starts, the short chains orient at first and the in situ silica phases also start to be deformed as shown in Fig. 5c. With the increase in oriented chains upon further stretching, the crystallites are generated in the rubber phases as shown in Fig. 5d. Under the large deformation, the silica filler network is broken down. Since there are different sizes of rubber phases, the collapse of silica layers occurs successively. Upon further deformation, the silica filler networks are totally broken down and the SIC are promoted similarly with the conventionally filler filled composites as shown in Fig. 5e. Here, the cartoons are drawn in order to emphasize the variation of one biphasic structure with a silica phase around a rubber phase. In reality, this type of deformation should be taken into account for all rubber phases of different sizes.

Appearance of the stepwise SIC is concluded to be due to the size distribution of the rubber particles in highly ammoniated NR latex. Recently, a dual crystallization behavior was reported in NR-based nanocomposite systems, where nanofiller with a high aspect ratio, e.g., nanoclay [43] and carbon nanotube [44], were used. Differently with these studies, a few steps of SIC shown in Fig. 4 were detected relating with the characteristic feature of the "NR latex template method" combining with the sol–gel reaction of TEOS [31]: The rubber particles in the latex got closer during drying the composite latex, and consequently, the densely packed in situ generated silica was dispersed around the rubber particles like a boundary layer.

In terms of onset strain of SIC, S-NR-Si showed a crystalline diffraction peak at the lower strain ($\alpha_{e, c}$=~2.25) than that of S-NR ($\alpha_{e,c}$=~3.5) as shown in Fig. 4c. The introduction of in situ silica apparently accelerated the start of SIC to result in the short induction period of SIC similarly with the composites prepared by a mechanical milling technique [21–23, 27–30]. The smaller onset strain of SIC of the reinforced systems is ascribed to two phenomena: The decrease of the volume fraction of rubbery phase at first and the high interfacial interaction between reinforcing fillers and rubbery matrix in the second. The former is a volume effect in general when filled, and the latter is dependent on the kind of mixed filler. However, the effective stretching ratio is used for the SIC analyses in this study. Therefore, the small $\alpha_{e,c}$ value of S-NR-Si suggests the presence of strong interfacial interaction between in situ silica and the rubber phases.
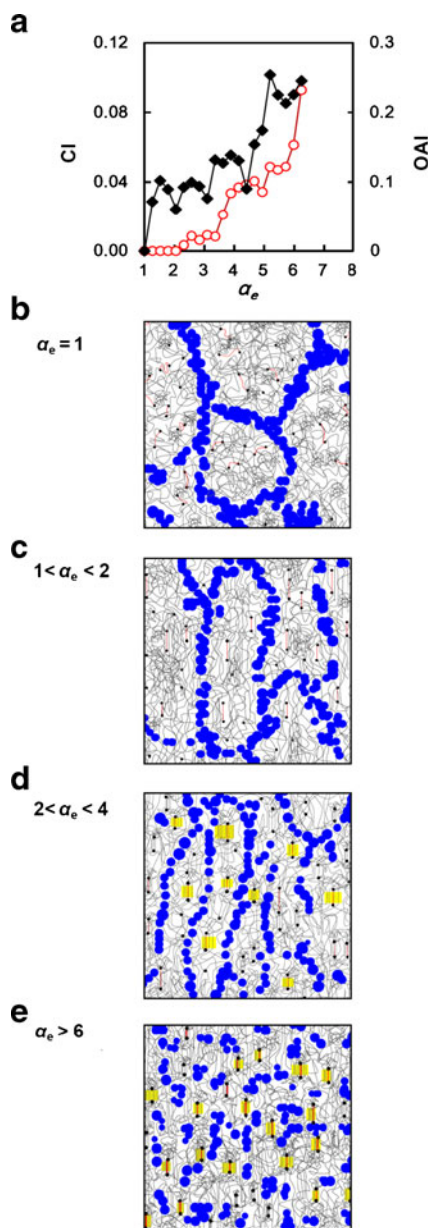
Fig 5 Variations of OAI and CI plotted against effective stretching ratio for S-NR-Si (**a**), and its speculated SIC behavior (**b**–**e**). This deformation occurs in each different sized rubber phase in the sulfur cross-linked in situ silica filled NR composite

Uncross-linked in situ silica filled NR composite

In general, a cross-linking significantly affects the SIC of NR [18, 19, 24, 26]. Since S-NR-Si is a cross-linked sample, the uncross-linked in situ silica filled composite (NR-Si) was subjected to the SIC study in order to highlight the effect of in situ silica phase on the SIC of NR in the composite. Strain dependences of OI, OAI, and CI of NR-Si are shown with those of S-NR-Si in Fig. 4d–f. It is worth noting that network chains oriented only a little upon stretching up to 2.0 of α_e in NR-Si. At the strain region of $2<\alpha_e<3$, both OI and OAI

increased and show a small plateau region. From about 3 of α_e, both values increased again upon further stretching, and their variations became small around 4.5 of α_e, where a small down was also observed. A shape of variation of CI in NR-Si was quite similar with that in S-NR-Si, although the variation in NR-Si began at a lower strain than S-NR-Si and the plateau regions were imperfect.

Comparing the SIC of NR-Si with that of S-NR-Si, a tendency of slower increases of OI and OAI was observed in the former than in the latter. Due to the absence of cross-linking sites in NR-Si, the orientation of NR chains became slower and its degree was lower in NR-Si than in S-NR-Si. Unexpectedly, however, the SIC of NR-Si was found to give higher CI values than that of S-NR-Si as shown in Fig. 4f. As reported previously, the in situ silica located at the surface not in the rubber phase [31]. Therefore, the pure rubber phases inside of silica phases in NR-Si are considered to be more crystallisable upon stretching comparing with S-NR-Si. This phenomenon clearly shows one of the roles of cross-linking sites to prevent the SIC, although the cross-linking sites are also known to accelerate the SIC. This observation may be of use for a material design of high performance rubber products. In terms of onset strain of SIC, the difference between the two composites was minor as shown in Fig. 4f in contrast to the observation above, i.e., cross-linked or not shows less influence. The interaction between NR and in situ silica may be related with the first orientation of rubber chains.

SIC of sulfur cross-linked NR prepared by the soft processing method

Form the viewpoint of the preparation method, the SIC of S-NR is also interesting because a majority of nonrubber components presents on the surface of rubber particles in the NR latex. Consequently, a specific morphology seems to be also formed in S-NR as reported earlier [5]. As shown in Fig. 4a–c, an effect of the nonrubber components around the rubber phases on the SIC was observed as expected. A tendency of SIC at $\alpha_e<\sim4$ in S-NR was similar with that in S-NR-Si, although the OI and OAI at each strain were considerably smaller than those of S-NR-Si. In addition, an orientation of rubber chains occurred at higher strain comparing with S-NR-Si. In S-NR, there is no silica layer in the interface between the rubber phases. As a result, the interaction between the nonrubber components is supposed to be weaker than that of in situ silica particles to result in these different SIC phenomena. It is also noted that the CI values at the first plateau of S-NR were almost same with those of S-NR-Si. This observation suggests that the smallest size of the rubber phase in S-NR is comparable with that of S-NR-Si. However, the steps of CI became less recognizable upon further stretching, which may be due to the weak interaction among the nonrubber components around the rubber phases in S-NR. This characteristic

Fig. 6 Relationship between apparent crystallite sizes, L_{200} (**a**) and L_{120} (**b**), and orientational fluctuation (**c**) against effective stretching ratio for S-NR-Si, NR-Si, and S-NR. The *lines* are connected between the data points
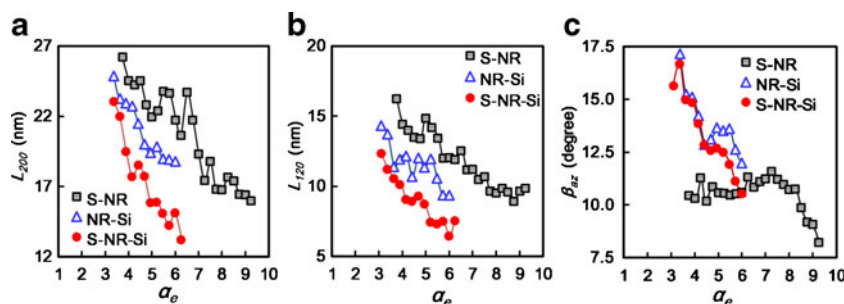
SIC of the unfilled NR latex vulcanizate is also a first report as far as we know. Note that Che et al. [20] studied on SIC for cross-linked NR films prepared from NR latex. However, their results did not show any stepwise SIC. It may be due to the different experimental conditions of the WAXD measurements. In their case, the image acquisition time for each scan was 30 s, and the samples were stretched at stretching speed of 10 mm/min. In our WAXD measurements in BL-40XU beamline at SPring-8, on the other hand, the incident beam was exposed on the sample for 40 ms every 3 s under the stretching speed of 100 mm/min. Therefore, it is believed that this experimental condition enabled us to find the unique SIC of the NR latex vulcanizates reflecting the specific structure ascribable to the rubber particles in the latex.

Characteristics of crystallites generated by SIC

In order to clarify the stepwise SIC behavior in more details, a few crystalline structural parameters, i.e., lateral crystallite sizes, fluctuation parameters, and lattice constants, were semi-quantitatively evaluated, and their results are shown in Fig. 6 and 7. The results are reliable as we obtained a good reproducibility among three fittings for all parameters. Errors among the three fittings for each point were found within ±0.8 % from the each average. Thus, the average values were plotted in the figures. Interestingly, a few steps were also observed in strain dependences of some structural parameters though not so marked as observed in Fig. 4. Upon stretching, lateral crystallite sizes, L_{200} and L_{120} of S-NR varied downward with ups and downs as shown in Fig. 6a and b, respectively. This tendency was also observed in S-NR-Si and NR-Si, although the tendency of ups and downs was reduced. The in situ silica

filling resulted in the smaller L_{200} and L_{120} than those of S-NR. The effect of sulfur cross-linking on L_{200} and L_{120} in S-NR-Si was also clearly detected, where the L_{200} and L_{120} values decreased.

In terms of orientation fluctuation (β_{az}) shown in Fig. 6c, the fluctuation degree became smaller upon stretching in the composites. The in situ silica phase disturbed the orientation of crystallites at the low strain. Differently with the in situ silica filling, the effect of sulfur cross-linking on β_{az} was small as shown in the variation of β_{az} in S-NR. The small variation up to $\alpha_e=\sim8$ suggests that not only the sulfur cross-linking sites but also the nonrubber components in NR were not so influential on the β_{az}, probably due to their flexibility comparing with the silica phases. This result also supports the presence of specific morphology in S-NR, which was obtained by soft processing technique [5].

An estimation of crystallite size in the direction parallel to the stretching was not easy. Thus, an average volume and number of strain-induced crystallites were not evaluated in this study. However, we believe that the orientational fluctuations of the crystallites are related to the crystallite size [16]. In the rubber phase surrounded by the silica layer, the development of the fluctuations due to the bending of lamellar crystal is supposed to easily occur during the crystal growth upon stretching. However, the β_{az} values of S-NR-Si and NR-Si varied downward upon stretching as shown in Fig. 6c, even though the small increase and short plateau regions were observed. Therefore, it is conceivable that the depression of β_{az} was ascribed to the decrease in crystallite size. In fact, the lateral sizes of S-NR-Si and NR-Si varied downward upon stretching as shown in Fig. 6a and b. Thus, the volume of strain-induced crystallites is speculated to be decreased by in situ silica filling, but the

Fig. 7 Variations of lattice constants of crystallites against effective stretching ratio for S-NR-Si, NR-Si and S-NR. *a* axis(**a**), *b* axis (**b**), *c* axis (**c**), and volume of the unit cell (**d**). The *lines* are connected between the data points
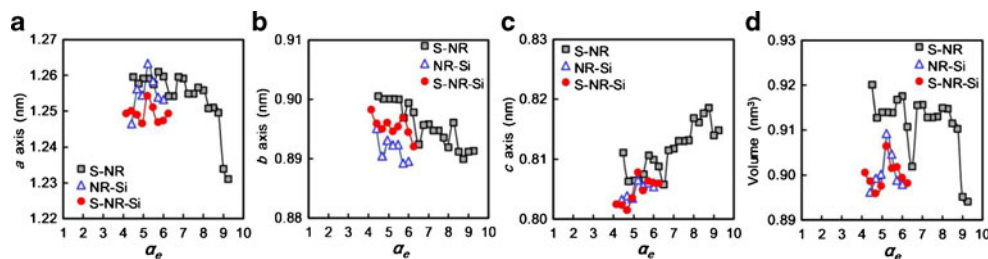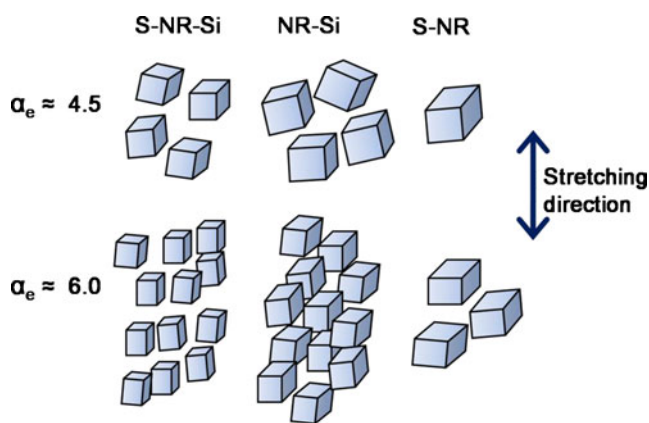
Fig 8 Speculated difference on the shapes and numbers of the strain-induced crystallites for S-NR-Si, NR-Si, and S-NR. Note that the *in situ* silica and the oriented and un-oriented amorphous chains are not displayed and the difference is relative

number of the crystallites is predicted to be increased oppositely because the CI values of S-NR-Si and NR-Si up to $\alpha_e = \sim4.5$ were larger than that of S-NR. The sulfur cross-linking sites in the composites may also work as perturbation sites for β_{az}. Therefore, the average volume of strain-induced crystallites over $\alpha_e = 4$ may be smaller in S-NR-Si than in NR-Si.

The effect of specific biphasic structured morphology was also observed in the strain dependence of lattice constants of the strain-generated crystallites as shown in Fig. 7a–c. A strain dependence of volume calculated from three lattice constants is also shown in Fig. 7d. Note that an orthorhombic unit cell according to the report by Nyburg [45] was used for the calculation. Only the results over $\alpha_e = 4$ are plotted with an accuracy. From Fig. 7, the following observations are extracted: The unit cells of each crystallite in all samples did not deform linearly with the strain, but the pure rubber phase inside the biphasic structures did not bring about a large variation on the lattice constants up to the high strain. The lattice constants contracted along the *b* direction (perpendicular to the stretching direction) and elongates in the *c* direction (parallel to the stretching direction) with small ups and downs in the both directions. Variations of lattice constant along the *a* direction are unique especially in S-NR-Si and NR-Si as shown in Fig. 7a. When the variations are compared with those of CI,

the increases of the lattice constants are found to be ascribable to the collapse of silica layers around the rubber phases. The ups and downs of other lattice constants and volume of the unit cell of strain-induced crystallites of NR were also related to the stepwise SIC phenomena. Not only the in situ silica filling but also the sulfur cross-linking affected the deformation of the unit cell of strain-induced crystallites of NR in the specific biphasic structured composites prepared from in situ silica and NR latex.

### Relationship between SIC and tensile properties of in situ silica filled NR composites

All the results so far described in this paper revealed that the in situ silica filled biphasic structure brought about a unique SIC behavior. Correspondingly, the observed SIC behaviors must be related to the tensile characteristics of the composites. The effects of in situ silica filling and sulfur cross-linking on tensile stress of the biphasic structured silica filled NR composites are discussed in this section.

Effect of in situ silica filling

As mentioned earlier, the tensile curve of S-NR-Si had different characteristics from that of S-NR. The biphasic structure was found to increase OAI to result in the promotion of SIC, where a generation of smaller crystallites was dominantly produced compared with the unfilled sample. Images for the generated crystallites are schematically shown in Fig. 8. Note that only crystallites are illustrated in this figure for the comparison, where the unoriented and oriented amorphous segments and in situ silica are not shown between the crystallites. Since we tentatively used the Nyburg's model for the unit cell of strain-induced crystallites of NR in this study, rectangular typed crystallites were assumed to be formed by SIC [45, 46]. Interestingly, a recent publication on the SIC of NR at −50 °C reported a model of the average crystallite size by using a novel two-dimensional WAXD simulation method, where rectangular typed crystallites were shown [47].

As shown in Fig. 8, the smaller crystallites may work as a nanofiller to reinforce the composites besides the in situ silica.

Fig. 9 Variations of OI (**a**), OAI (**b**), and CI (**c**) plotted against tensile stress for S-NR-Si, NR-Si, and S-NR
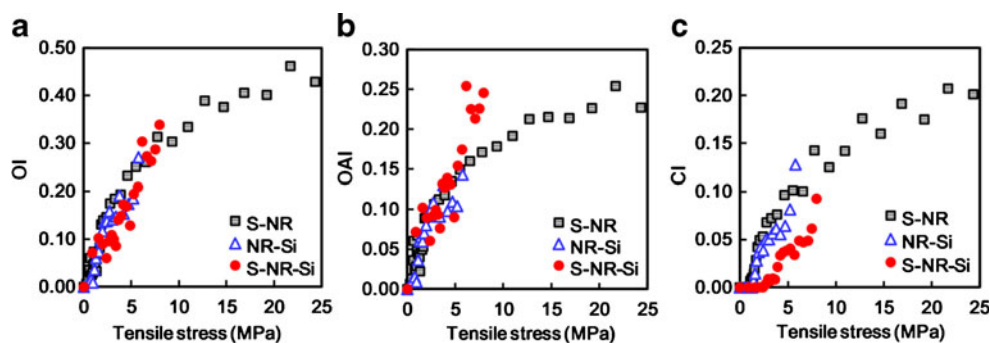
The reinforcement effect by in situ silica must be dominant at the lower strain, and the role of strain-induced crystallites as the nanofiller is supposed to be increasing with the increase in strain. At the high strain, both in situ silica and generated crystallites must bear the stress with the oriented amorphous segments. Therefore, the OAI became approximately twice compared with that at the low strain. The large OAI may have been derived from the pure rubber phases in the biphasic structure. For an example, the CI values were comparable between in S-NR-Si and S-NR at $4<\alpha_e<7$, but the OAI was much larger in S-NR-Si than in S-NR. Consequently, the higher stress at lower strain was achieved in S-NR-Si. The orientation of the crystallites in S-NR-Si became better with the increase in strain and became comparable with that of S-NR, which also contributed to the increase in stress.

As reported previously, the in situ silica is estimated to be scarcely contained inside the rubber particles [31]. Therefore, the results on NR-Si and S-NR-Si in this article may be useful to reveal an effect of "filler network" on SIC. A term of "filler network" shows more or less continuously aggregated or agglomerated fillers in rubber matrix, which has been believed to be the origin of reinforcement effect by filler in polymer science and technology [42]. However, it has been difficult to prepare a model composite. Recently, a weblike structure of reduced graphene oxide was reported as a model of filler network [48]. Our novel biphasic structured soft composites, however, may be more preferable for explaining the characteristics of the filler network because the in situ silica is particulate and similar with conventional nanofillers such as carbon black and silica in terms of their shapes. The effect of the silica phase on the stress is also clearly observed in Fig. 9, where stress dependences of OI, OAI, and CI are shown. It appears that the strain-induced crystallites worked as the secondary reinforcer after the primary reinforcer, in situ silica. The role of oriented amorphous chains was also found to be important to transfer the stress between the reinforcers.

Effect of sulfur cross-linking

When S-NR-Si and NR-Si are compared, it is found that the OI and OAI increased by sulfur cross-linking, but the CI oppositely decreased as shown in Fig. 4. In addition, the size of strain-induced crystallites became smaller by cross-linking. Therefore, the increase in stress by cross-linking shown in Fig. 3 is ascribed to the significant increase in OAI, which may play a role to transfer the load to the silica and the small crystallites. The high orientation of the crystallites in S-NR-Si than in NR-Si shown in Fig. 6c may also promote the transfer, which was clearly observed over $\alpha_e=\sim4$. The effect of large *OAI* on the stress was more apparently observed in Fig. 9b.

Conclusions

The time-resolved WAXD measurement during stretching revealed that the SIC of the biphasic structured in situ silica filled NR soft composites occurred stepwise, i.e., the degree of crystallinity showed the repetition of increase and standstill cycles. This behaviour was found on the composites prepared from NR latex with in situ silica by using the liquid-state mixing and casting methods. The unfilled NR latex vulcanizate prepared by casting also showed the stepwise SIC, although the steps became obscured with the increase in strain. The presence of new biphasic structure in the NR latex vulcanizate brought about the increase in oriented amorphous chains to result in the promotion of SIC, where the generation of small crystallites dominantly occurred stepwise due to the silica phases around the rubber phases. The small crystallites worked as nanofillers to reinforce NR via the oriented amorphous chains. Since the in situ silica was not introduced inside the rubber phases but on the surface, the observed characteristic phenomena of the SIC may be of interest in understanding a role of filler network for the reinforcement of rubber. The role has been one of the big questions in rubber science and technology because the ideal model composite only with filler networks has been difficult to be prepared. For further development of rubber science, a study on the biphasic structured NR composites with different silica contents will be necessary from the viewpoints of silica contents and cyclic deformation, which will be reported in a near future.

References

1. Bateman L (1963) The chemistry and physics of rubber-like substances. MacLaren, London
2. Roberts AD (1988) Natural rubber science and technology. Oxford Science, Oxford
3. Jones KP, Allen PW (1992) Historical development of the world rubber industry. In: Sethuraj MR, Mathew NM (eds) Developments in crop science, vol 23. Natural rubber: biology, cultivation and technology. Elsevier, Amsterdam, pp 1–22
4. Rodgers B, Waddell W (2005) The science of rubber compounding. In: Mark JE, Erman B, Eirich FR (eds) The science and technology of rubber, 3rd edn. Elsevier Academic, Oxford
5. Blackley DC (1997) Polymer lattices science and technology, vol 2: types of lattices, 2nd edn. Chapman & Hall, London

6. Wititsuwanakul D, Wititsuwanakul R, Steinbuchel A (2001) Biopolymers, vol 2. Wiley-VCH, Weinheim

7. Katz JR (1925) Röntgenspektrographische Untersuchungen am gedehnten Kautschuk und ihre mögliche Bedeutung für das Problem der Dehnungseigenschaften dieser Substanz. Naturwiss 19:410–418

8. Flory PJ (1953) Principles of polymer chemistry. Cornell University, Ithaca

9. Treloar LRG (1975) The physics of rubber elasticity. Clarendon, Oxford

10. Mitchell GR (1984) A wide-angle X-ray study of the development of molecular orientation in crosslinked natural rubber. Polymer 25: 1562–1572

11. Mandelken L (2002) Crystallization of polymers, vol 1: equilibrium concepts, 2nd edn. Cambridge University Press, Cambridge

12. Andrews EH (1962) Spherulite morphology in thin films of natural rubber. Proc R Soc A 270:232–241

13. Tsuji M, Kohjiya S (1995) Structural studies on crystalline polymer solids by high-resolution electron microscopy. Prog Polym Sci 20: 259–308

14. Murakami S, Senoo K, Toki S, Kohjiya S (2002) Structural development of natural rubber during uniaxial stretching by *in situ* wide angle X-ray diffraction using a synchrotron radiation. Polymer 43: 2117–2120

15. Toki S, Sics I, Ran S, Liu L, Hsiao BS, Murakami S, Senoo K, Kohjiya S (2002) New insights into structural development in natural rubber during uniaxial deformation by *in situ* synchrotron X-ray diffraction. Macromolecules 35:6578–6584

16. Tosaka M, Murakami S, Poompradub S, Kohjiya S, Ikeda Y, Toki S, Sics I, Hsiao BS (2004) Orientation and crystallization of natural rubber network as revealed by WAXD using synchrotron rRadiation. Macromolecules 37:3299–3309

17. Tosaka M, Kohjiya S, Murakami S, Poompradub S, Ikeda Y, Toki S, Scis I, Hsiao BS (2004) Effect of network-chain length on strain-induced crystallization of NR and IR vulcanizates. Rubber Chem Technol 77:711–723

18. Ikeda Y, Yasuda Y, Makino S, Yamamoto S, Tosaka M, Senoo K, Kohjiya S (2007) Strain-induced crystallization of peroxide-crosslinked natural rubber. Polymer 48:1171–1175

19. Ikeda Y, Yasuda Y, Hijikata K, Tosaka M, Kohjiya S (2008) Comparative study on strain-induced crystallization behavior of peroxide cross-linked and sulfur cross-linked natural rubber. Macromolecules 41:5876–5884

20. Che J, Toki S, Valentin JL, Brasero J, Nimpaiboon A, Rong L, Hsiao BS (2012) Chain dynamics and strain-induced crystallization of pre- and postvulcanized natural rubber latex using proton multiple quantum NMR and uniaxial deformation by *in situ* synchrotron X-ray diffraction. Macromolecules 45:6491–6503

21. Poompradub S, Tosaka M, Kohjiya S, Ikeda Y, Toki S, Sics I, Hsiao BS (2005) Mechanism of strain-induced crystallization in filled and unfilled natural rubber vulcanizates. J Appl Phys 97:103529/1–103529/9

22. Ikeda Y, Kato A, Shimanuki J, Kohjiya S, Tosaka M, Poompradub S, Toki S, Hsiao BS (2007) Nano-structural elucidation in carbon black loaded NR vulcanizate by 3D-TEM and *in situ* WAXD measurements. Rubber Chem Technol 80(2):251–264

23. Ikeda Y (2005) Green nano-composites prepared from natural rubber and *in situ* silica. Kautsch Gummi Kunstst 58:455–460

24. Ikeda Y, Higashitani N, Hijikata K, Kokubo Y, Morita Y, Shibayama M, Osaka N, Suzuki T, Hitoshi E, Kohjiya S (2009) Vulcanization: new focus on a traditional technology by small-angle neutron scattering. Macromolecules 42:2741–2748

25. Karino T, Ikeda Y, Yasuda Y, Kohjiya S, Shibayama M (2007) Nonuniformity in natural rubber as revealed by small-angle neutron scattering, small-angle X-ray scattering, and atomic force microscopy. Biomacromolecules 8:693–699

26. Suzuki T, Osaka N, Endo H, Shibayama M, Ikeda Y, Asai H, Higashitani N, Kokubo Y, Kohjiya S (2010) Nonuniformity in cross-linked aatural rubber as revealed by contrast-variation small-angle neutron scattering. Macromolecules 43(3):1556–1563

27. Gehman SD, Field JE (1941) X-ray structure of rubber-carbon black mixtures rubber. Chem Technol 14:85–97

28. Trabelsi S, Albouy PA, Rault J (2003) Effective local deformation in stretched filled rubber. Macromolecules 36(24):9093–9099

29. Chenal JM, Gauthier C, Chazeau L, Guy L, Bomal Y (2007) Parameters governing strain induced crystallization in filled natural rubber. Polymer 48:6893–6901

30. Dupres S, Long DR, Albouy PA, Sotta A (2009) Local deformation in carbon black-filled polyisoprene rubbers studied by NMR and X-ray diffraction. Macromolecules 42:2634–2644

31. Tohsan A, Phinyocheep P, Kittipoom S, Pattanasiriwisawa W, Ikeda Y (2012) Novel biphasic structured composite prepared by *in situ* silica filling in natural rubber latex. Polym Adv Technol 23:1335–1342

32. Mark JE, Pan SJ (1982) Reinforcement of poly(dimethylsiloxane) networks by *in situ* precipitation of silica: a new method for preparation of filled elastomers. Makromol Che Rapid Commun 3:681–685

33. Brinker CJ, Scherer GW (1990) Sol–gel science: the physics and chemistry of sol–gel processing. Academic, New York

34. Kohjiya S, Ikeda Y (2000) Reinforcement of general-purpose grade rubbers by silica generated *in situ*. Rubber Chem Technol 73:534–550

35. SPring-8 Web site. http://www.spring8.or.jp/en/

36. Hahn T (1983) International tables for crystallography, vol A. Reidel, Holland

37. Scherrer P (1918) Estimation of the size and internal structure of colloidal particles by means of Röntgen rays. Gottinger Nachrichten 2:96–100

38. Klug HP, Alexander LE (1974) X-ray diffraction procedures for poly-crystalline and amorphous materials, 2nd edn. Wiley-Interscience, New York

39. Bokobza L (2001) Reinforcement of elastomeric networks by fillers. Macromol Symp 169:243–260

40. Ikeda Y, Kato A, Shimanuki J, Kohjiya S (2004) Nano-structural observation of *in situ* silica in natural rubber matrix by three dimensional transmission electron microscopy. Macromol Rapid Commun 25:1186–1190

41. Kohjiya S, Kato A, Shimanuki J, Hasegawa T, Ikeda Y (2005) Three-dimensional nano-structure of *in situ* silica in natural rubber as revealed by 3D-TEM/electron tomography. Polymer 46:4440–4446

42. Kohjiya S, Kato A, Ikeda Y (2008) Visualization of nanostructure of soft matter by 3D-TEM:Nanoparticles in a natural rubber matrix. Prog Polym Sci 33:979–997

43. Gonzlez JC, Retso H, Verdejo R, Toki S, Hsiao BS, Emmanuel P, Miguel AL (2008) Effect of nanoclay on natural rubber microstructure. Macromolecules 41:6763–6772

44. Weng G, Huang G, Qu L, Nie Y, Wu J (2010) Large-scale orientation in a vulcanized stretched natural rubber network: proved by *in situ* synchrotron X-ray diffraction characterization. J Phys Chem B 114: 7179–7188

45. Nyburg SC (1954) A statistical structure for crystalline rubber. Acta Crystallogr 7:385–392

46. Huneau B (2011) Strain-induced crystallization of natural rubber: A review of X-ray diffraction investigations. Rubber Chem Technol 84: 425–452

47. Che J, Burger C, Toki S, Rong L, Hsiao BS, Amnuaypornsri S, Sakdapipanich J (2013) Crystal and crystallites structure of natural rubber and synthetic cis-1,4-polyisoprene by a new two dimensional wide angle X-ray diffraction simulation method. I. Strain-induced crystallization. Macromolecules 46:4520–4528

48. Potts JR, Shankar O, Du L, Ruoff RS (2012) Processing–morphology–property relationships and composite theory analysis of reduced graphene oxide/natural rubber nanocomposites. Macromolecules 45: 6045–6055